Int. J. Electrochem. Sci., 17 **(2022)** Article Number: 220743, doi: 10.20964/2022.07.42

International Journal of
ELECTROCHEMICAL
SCIENCE
www.electrochemsci.org

Dimocarpus longan Lour Leaf Extract as Green Corrosion Inhibitor for Copper in Sulfuric Acid Solution

Lixia Cao

The Chinese Society for Metals, Beijing 100081, China
E-mail: caolixiacsm@163.com

Received: 16 March 2022 / *Accepted:* 4 May 2022 / *Published:* 6 June 2022

In this work, the Dimocarpus longan Lour Leaf Extract (DLLE) was obtained by soaking in sulfuric acid solution. Dimocarpus longan Lour Leaf Extract contains 3,4,5-Trihydroxybenzoic acid ethyl ester (TBE), 3,4,5,7-Tetrahydroxyflavone (TDF) and 3,3',4', 5,7-Pentahydroxyflavone2-(3 ,4-Dihydroxyphenyl)-3,5,7-trihydroxy-4H-chromen-4-one (PDH). The experimental and theoretical calculation results show that the DLLE can exhibit excellent corrosion inhibition performance. As the concentration of DLLE increases, the corrosion inhibition performance increases significantly. When the concentration of DLLE reaches 400 mg/L, its corrosion inhibition efficiency can reach about 98% at 318 K. Quantum chemical calculation results show that TBE, TDF and PDH in DLLE have large dipole moments and small energy gap values. All these indicate that the DLLE can exhibit high corrosion inhibition performance. Molecular dynamics simulations show that TBE, TDF and PDH can be adsorbed on the Cu (111) surface in parallel with high adsorption energy. Therefore, both experimental and theoretical calculation results demonstrate that the DLLE can exhibit high corrosion inhibition performance.

Keywords: Plant extracts, Electrochemical tests, Quantum chemical calculations, Molecular dynamics simulations, Binding energy

1. INTRODUCTION

The corrosion reaction of metal materials is an unavoidable process. The contact of metal materials with corrosive media in the surrounding environment during service will cause great corrosion of metal materials. When the instruments and equipment of metal materials are eroded by corrosive corrosive media, it will not only cause huge economic losses and bring serious hidden dangers to safety. Therefore, the research on corrosion protection of metal materials is particularly important. Among many corrosion protection methods, corrosion inhibitor has more prominent advantages, such as it has the characteristics of small amount and remarkable effect, high cost performance, simple use and other series of advantages [1-5]. Therefore, it has become one of the important methods in corrosion protection

methods. Organic corrosion inhibitors usually contain heteroatoms such as nitrogen, sulfur, and oxygen, as well as conjugated bonds [6-13]. However, traditional organic corrosion inhibitors have some fatal defects in the use process, such as poor solubility, strong taste, and pollution of the ecological environment. Therefore, it is particularly important to develop green and efficient corrosion inhibitors.

In recent years, a large number of corrosion protection scientists have developed a series of environmentally friendly and efficient corrosion inhibitors, involving amino acids, flavors, ionic liquids and plant extracts, etc. Among them, the research of plant extracts as corrosion inhibitors is still important. In recent years, a large number of corrosion protection scientists have carried out related research on plant corrosion inhibitors. Tan et al. [14] studied the corrosion inhibition performance of betel leaf water extract on Q23 steel in hydrochloric acid solution. The electrochemical data showed that betel leaf water extract can effectively inhibit the corrosion of Q235 steel, and with the increase of temperature, betel leaf water extract can still maintain high corrosion inhibition efficiency. Feng et al. [15] studied the corrosion inhibition performance of Veratrum root extract on copper in sulfuric acid solution. When the concentration of Veratrum root extract was 200 ppm, the corrosion inhibition efficiency could reach more than 97%. And they explained the corrosion inhibition mechanism of Veratrum root extract in detail in the manuscript. Guo et al. [16] studied the corrosion inhibition performance of Banana leaves water extracts on X70 steel in hydrochloric acid solution, Infrared experimental data show that banana leaf extract contains a large number of heteroatomic compounds. The experimental data show that in a certain temperature range, with the increase of banana leaf extract concentration, the corrosion inhibitor can still show high corrosion inhibition performance.

In this work, a large number of papers are referenced, and 0.5 M sulfuric acid solution is selected as the corrosion test medium[17-19], 0.5 M sulfuric acid solution was used as the extract to obtain the DLLE, and the obtained DLLE had good solubility and high corrosion inhibition efficiency. And many experimental methods such as electrochemical method, surface topography analysis and theoretical calculation were used in the manuscript to ver ify the high corrosion inhibition performance of DLLE on copper in sulfuric acid medium.

2. EXPERIMENTAL

2.1 Materials

After the Dimocarpus longan Lour leaves are collected, they are washed with ultrapure water. After cleaning, the Dimocarpus longan Lour leaves were pulverized and dried, and placed in a beaker containing 0.5 M sulfuric acid solution for 36 hours. Then, the supernatant is poured into a small beaker for freeze-drying to obtain the target corrosion inhibitor, which is placed in a desiccator for use. Dimocarpus longan Lour leaves were dissolved in 0.5 M sulfuric acid solution to prepare a concentration gradient of 50 mg/L, 100 mg/L, 200 mg/L, and 400 mg/L. 0.5 M sulfuric acid solution as blank solution.

2.2 Fourier infrared spectroscopy test

Dimocarpus longan Lour leaves extract was tested using Fourier transform infrared spectroscopy in the range of 4000 cm^{-1} to 500 cm^{-1}. The results after the test are shown in Fig. 1. Among them, the

peak at 3273 cm^{-1} is caused by the stretching vibration of the -OH bond. The peak at 2917 cm^{-1} is caused by the stretching vibration of the -CH bond. The peak at 1602 cm^{-1} is caused by the C=C stretching vibration in the benzene ring. The peak at 1375 cm^{-1} is caused by -CH_3 stretching vibration. The peak at 1050 cm^{-1} is caused by the stretching vibration of the C-O bond. In addition, the reference [20] combined with the components of Dimocarpus longan Lour leaves extract show that longan leaves contain 3,4,5-Trihydroxybenzoic acid ethyl ester (TBE), 3,4,5,7-Tetrahydroxyflavone (TDF) and 3,3',4', 5,7-Pentahydroxyflavone2-(3,4-Dihydroxyphenyl)-3,5,7-trihydroxy-4H-chromen-4-one (PDH) three compounds. And their chemical structural formulas are listed in Fig. 2.

2.3 SEM test and electrochemical test

Grind the copper sample for SEM on 180-5000 grit sandpaper, the polished and bright samples were soaked in sulfuric acid solution containing 400 ppm and without corrosion inhibitor for 34 hours, and then the surface morphology was tested. Cut the copper sample to a size of 1×1×1 cm^3, leaving only one working surface exposed to the corrosive medium. The electrochemical test adopts the classic three-electrode system, and conducts open circuit potential test, electrochemical impedance spectroscopy test and potentiodynamic polarization curve test respectively. The range of polarization curve test is E_{OCP}±250 mV, and the polarization rate of the test is 2 mV/s.

2.4 Theoretical calculation

The three main components TBE, TDF and PDH in Dimocarpus longan Lour leaves extract were optimized using Materials Studio software.

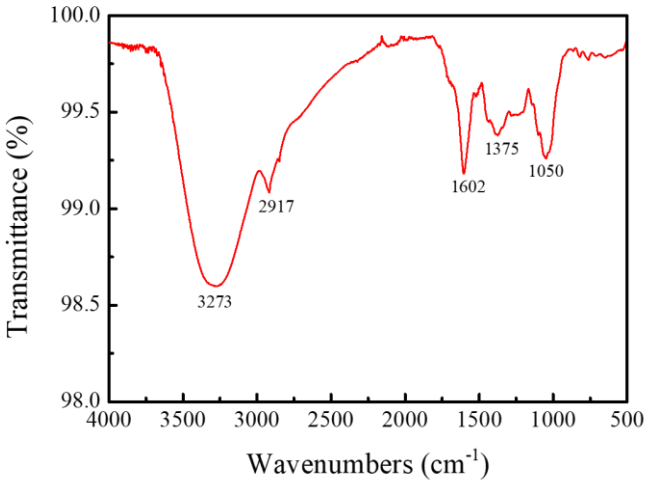

Figure 1. Fourier transform infrared spectrum of Dimocarpus longan Lour leaves.

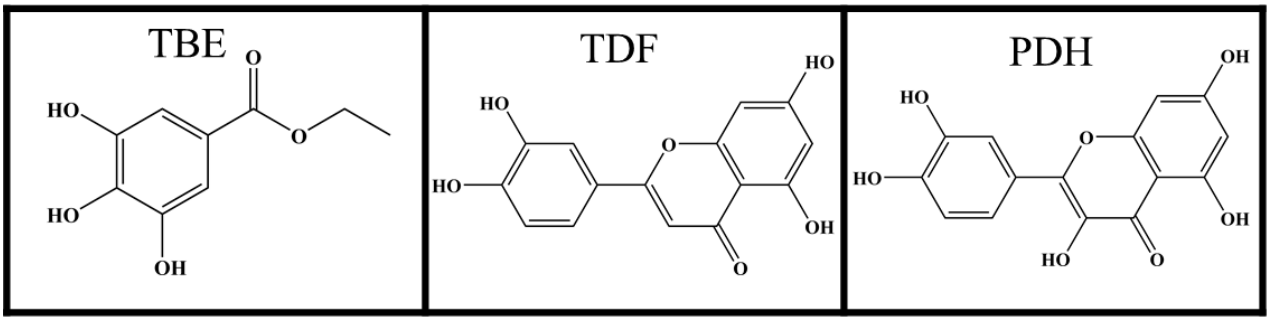

Figure 2. Three main components of longan leaf extract.

Their frontier molecular orbital distributions, energy gap values, dipole moments and electrostatic diagrams are calculated separately. And the Forcite module of Materials Studio software was used to simulate the adsorption behavior and binding energy of TBE, TDF and PDH on Cu(111) surface.The 600 water molecules and a inhibitor molecule were filled in this vacuum layer. Force field was selected COMPASS, and the time step is 1 fs. All the positions of Cu atoms are "freezing". The total simulation time was 800 ps.

3. RESULTS AND DISCUSSION

3.1 Potentiodynamic polarization curve

Figure 3 shows the potentiodynamic polarization curves of copper electrodes immersed in 0.5 M sulfuric acid solution containing different concentrations of Dimocarpus longan Lour leaves at a temperature of 318 K. As shown in Fig. 3, it can be clearly found that with the increase of the concentration of DLLE, the corrosion current density obviously shows a downward trend. This indicates that the DLLE can effectively inhibit the corrosion of copper in sulfuric acid medium after being adsorbed on the copper surface. In addition, it is worth mentioning that with the increase of the concentration of longan leaves, the decrease of the cathode branch is significantly greater than that of the anode, which indicates that the DLLE can effectively inhibit the precipitation of dissolved oxygen at the cathode after being adsorbed on the copper surface [21, 22]. In addition, after adding the DLLE, the value of the corrosion potential shifted to the cathode direction obviously, which also indicated that the DLLE could inhibit the reaction of the cathode.

The polarization curve parameters in Table 1 were obtained by Tafel extrapolation. These parameters include corrosion current density, corrosion potential, cathodic and anodic slope, and corrosion inhibition efficiency, respectively. The corrosion inhibition efficiency can be solved by the following formula [23-28]:

$$\eta(\%) = \frac{i_{corr,0} - i_{corr}}{i_{corr,0}} \times 100 \qquad (1)$$

where $i_{corr,0}$ and i_{corr} represent the corrosion current densities of unadded and added longan leaf extracts, respectively. It can be found that the value of the corrosion current density in the blank solution

is 18.86 μA cm^{-2}, When the concentration of longan leaf extract was 400 mg/L, the corrosion current density value decreased sharply to 0.39 μA cm^{-2}. At this time, the corrosion inhibition efficiency was 97.9%. The value of the corrosion potential in the blank solution was –49 mV, and the value of the corrosion potential after adding the corrosion inhibitor moved to the cathode direction obviously, but the change range was less than 85 mV, which indicated that the DLLE was a mixed corrosion inhibitor [29, 30]. The cathodic and anodic branches of the polarization curves were significantly altered after the addition of DLLE in sulfuric acid medium. This indicates that DLLE can effectively inhibit the corrosion of copper in sulfuric acid medium.

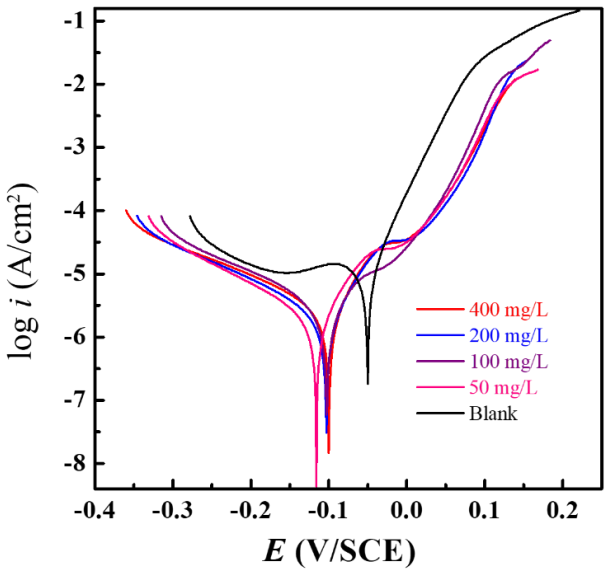

Figure 3. Potentiodynamic polarization curves of copper immersed in 0.5 M sulfuric acid medium containing different concentrations of DLLE at 298 K.

Table 1. Potentiodynamic polarization curves parameters of copper immersed in 0.5 M sulfuric acid medium containing different concentrations of DLLE at 298 K.

C (mg/L)	E_{corr}(mV/SCE)	i_{corr}(μA cm^{-2})	β_c(mV dec^{-1})	β_a(mV dec^{-1})	η(%)
Blank	–49	18.86	–209.4	80.7	—
DLLE					
50	–116	1.45	–206.4	62.1	92.3
100	–103	0.66	–187.3	87.7	96.5
200	–105	0.55	–193.5	72.9	97.1
400	–99	0.39	–182.9	69.5	97.9

3.2. Electrochemical impedance spectroscopy test

Fig. 4(a) and (b) show Nyquist plot and Bode plot of copper electrode immersed in sulfuric acid corrosion medium, respectively. It can be found that with the increase of DLLE concentration, the radius of the capacitive reactance arc in the Nyquist plot increases significantly, which indicates that DLLE can increase the charge transfer resistance after adsorption on the copper surface. In the blank solution without DLLE, it can be found that the capacitive reactance arc has an upward curve from the low frequency region. This is caused by the diffusion of copper ions after corrosion on the surface of the copper electrode into the corrosion medium. In Fig. 4(b), the phase angle is obviously broadened after adding DLLE in the Bode diagram, which is due to the two relaxation processes generated by the adsorption of DLLE on the copper surface. One relaxation process is caused by the charge transfer resistance, and the other is caused by the desorption of DLLE on the copper surface[31, 32].

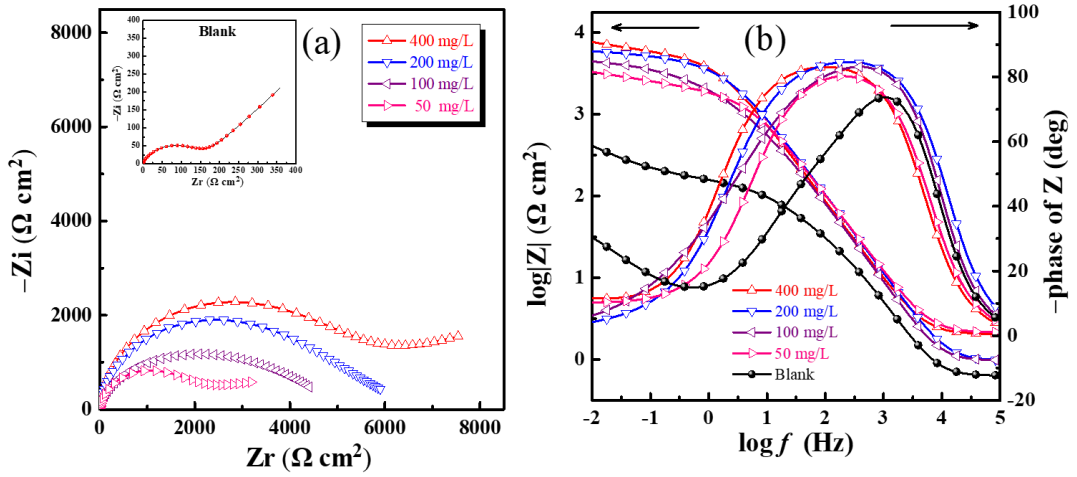

Figure 4. (a) Nyquist plot and (b) Bode graph of copper immersed in 0.5 M sulfuric acid medium containing different concentrations of DLLE at 298 K.

Table 2. Electrochemical impedance spectroscopy parameters of copper immersed in 0.5 M sulfuric acid medium containing different concentrations of DLLE at 298 K.

C	R_f	R_{ct}	R_p	C_f	n_1	C_{dl}	n_2	W	η (%)
(mg/L)	(kΩ cm^2)	(kΩ cm^2)	(kΩ cm^2)	(μF cm^{-2})		(μF cm^{-2})		(×10^{-2} Ω cm^2 s$^{1/2}$)	
Blank	0.01	0.13	0.14	143.1	0.98	119.7	0.64	1.3	—
DLLE									
50	0.05	2.11	2.16	69.1	1	71.2	0.67	—	93.5
100	0.11	4.82	4.93	54.3	0.99	60.1	0.65	—	97.1
200	0.15	5.91	6.06	43.6	0.97	47.1	0.59	—	97.7
400	0.22	7.12	7.34	33.3	1	35.4	0.67	—	98.1

The electrochemical impedance spectroscopy data in Table 2 are obtained by fitting the equivalent circuit diagram in Fig. 5. Fig. 5(a) is used to fit the electrochemical impedance spectroscopy data in the blank solution. Fig.5(b) is used to fit the electrochemical impedance spectroscopy data with DLLE. The *CPE* stands for the constant phase angle element, its definition as follow [33-35]:

$$\eta(\%) = \frac{R_P - R_{P,0}}{R_p} \times 100 \quad (2)$$

$$Z_{CPE} = \frac{1}{Y_0 (j\omega)^n} \quad (3)$$

$$C = Y_0(\omega)^{n-1} = Y_0(2\pi f_{Z_{im-Max}})^{n-1} \quad (4)$$

From Table 2, it can be found that with the increase of DLLE concentration, the membrane resistance R_f shows an increasing trend. This indicates that within a certain range, with the increase of DLLE concentration, the film formed on the copper surface is more dense. In addition, the values of C_f and C_{dl} decreased with the increase of corrosion inhibition efficiency, indicating that DLLE replaced the water molecules on the copper surface and adsorbed on the copper surface, thus forming a dense protective film[36, 37].

Table 3. Plant corrosion inhibitors of copper immersed in 0.5 M sulfuric acid solution in recent years.

Extracts	Metal	Corrosion Medium	Performance
Passiflora edulia Sims leaves [38]	Cu	0.5 M H_2SO_4	95.7% (800 mg/L)
Veratrum root [15]	Cu	0.5 M H_2SO_4	96.4% (250 mg/L)
Artocarpus heterophyllus Lam leaves [39]	Cu	0.5 M H_2SO_4	97.3% (500 mg/L)
Morinda citrifolia Linn leaves [40]	Cu	0.5 M H_2SO_4	96.3% (800 mg/L)
psidium guajava linn leaves [17]	Cu	0.5 M H_2SO_4	92.5% (600 mg/L)
Papaya leaves [31]	Cu	0.5 M H_2SO_4	92.5% (150 mg/L)

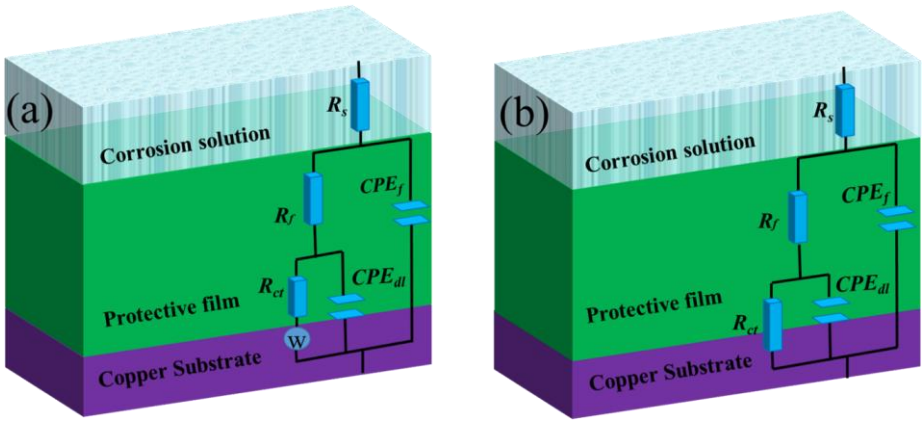

Figure 5. Equivalent circuit diagram for fitting electrochemical impedance spectroscopy: (a) with Warburg and (b) without Warburg.

Table 3 presents the papers on the corrosion inhibitor of copper in sulfuric acid solution by plant extracts in the last two years. After comparison, it can be found that when the concentration of DLLE reaches 400 mg/L, its corrosion inhibition efficiency can reach more than 98%, so it can be judged that DLLE is a high-performance corrosion inhibitor.

3.3. Quantum chemical calculations

Fig. 6 presents the optimized molecular structures and electrostatic diagrams of TBE, TDF and PDH, respectively. It can be found from the figure that the three molecules of TBE, TDF and PDH are basically on the same plane, which is due to the adsorption of corrosion inhibitors on the copper surface. In addition, the electrostatic diagrams of the three molecules of TBE, TDF and PDH consist of red and blue parts, which correspond to the electron-donating and electron-withdrawing abilities, respectively[41]. Fig. 7 shows the distribution of electron clouds in the HOMO and LUMO orbitals of TBE, TDF and PDH. From Fig. 7, it can be found that the electron clouds on their HOMO orbitals are almost distributed over the entire molecule, which indicates that these positions are favorable for electron-donating formation chemical adsorption[42]. The energy gap values of TBE, TDF and PDH are –1.23 eV, –1.38 eV, and –1.29 eV, respectively. The large dipole moment value and small energy gap value indicate that they both exhibit high corrosion inhibition performance.

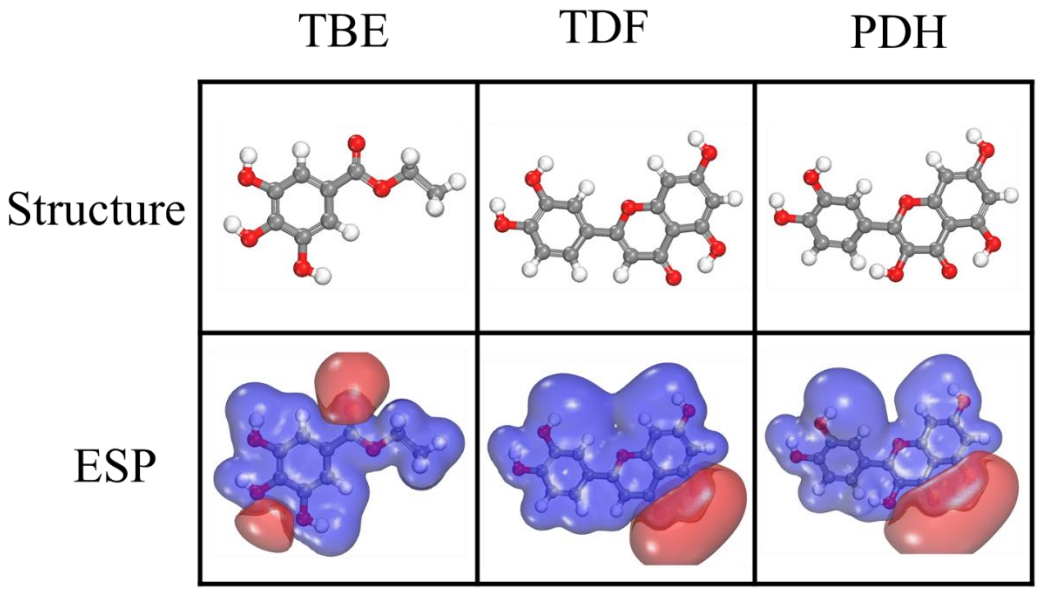

Figure 6. Molecular structures and electrostatic diagrams after optimization of TBE, TDF and PDH

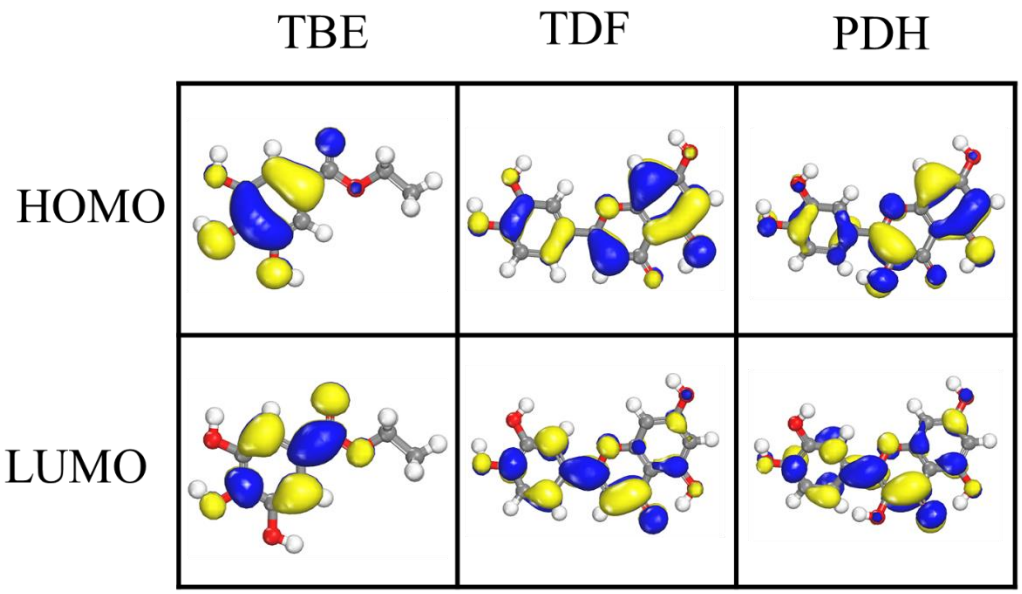

Figure 7. HOMO and LUMO orbital distributions of TBE, TDF and PDH

3.4. Molecular dynamics simulation

Fig. 8 presents the adsorption configurations of TBE, TDF and PDH on Cu(111) surface. As shown in Fig. 8, all three molecules can be adsorbed on the metal surface in parallel to obtain the maximum coverage.

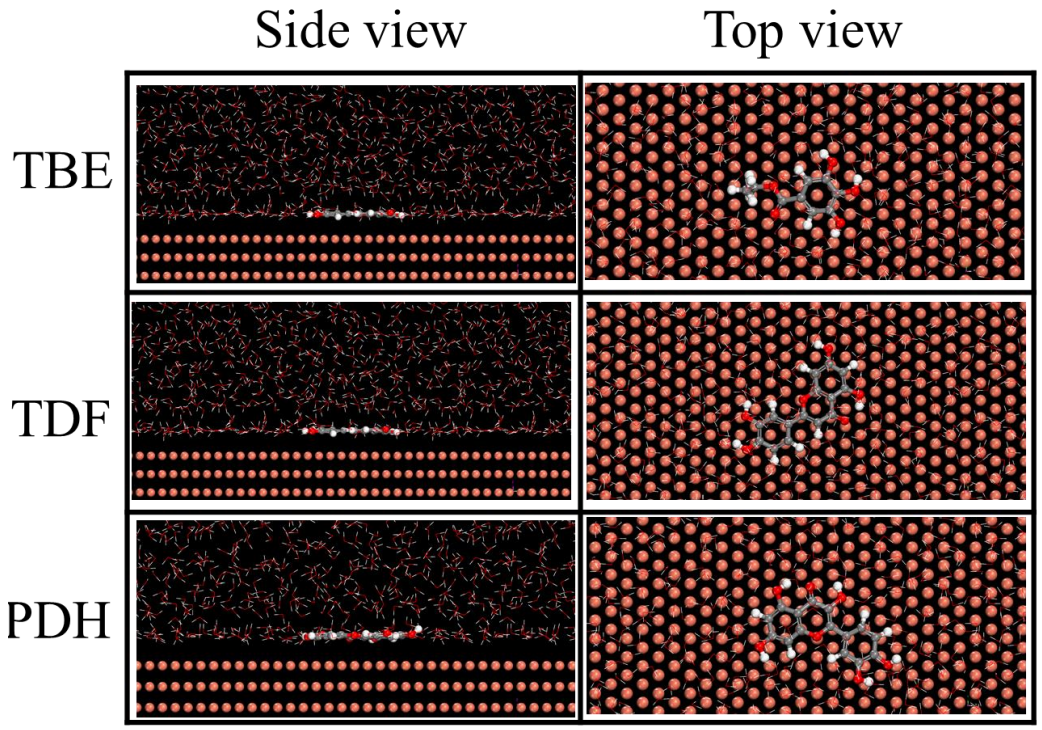

Figure 8. Adsorption configurations of TBE, TDF and PDH on Cu (111) surface

The binding energies of the three molecules on the copper surface can be calculated by the following formulas [43-45]:

$$E_{interact} = E_{tot} - (E_{subs} + E_{inh}) \quad (5)$$

$$E_{binding} = -E_{interact} \quad (6)$$

where $E_{binding}$ is the binding energy of system, E_{tot} stands for the total energy of the study system, E_{subs} is the energy of the researched system without inhibitor, E_{inh} is the TBE, TDF and PDH energy. After calculation, it can be known that the binding energies of TBE, TDF and PDH are –378.1 kJ/mol, –409.3 kJ/mol, and –428.4 kJ/mol, respectively. These data all indicate that DLLE can exhibit high corrosion inhibition performance.

3.5. Surface topography analysis

Fig. 9 presents the topography of the copper sample surface under different experimental conditions. Fig. 9(a) is the surface morphology in the blank solution. It can be found that after the copper sample was immersed in 0.5 M sulfuric acid solution for 34 hours, the entire copper surface was severely damaged, and the corrosion voids were very dense and uniform, showing a phenomenon of uniform corrosion. Fig. 9(b) is the surface topography of the entire copper sample after adsorption of DLLE. It can be clearly found that the copper surface is obviously flat after adding DLLE, the corrosion voids are small, and the scratches after grinding are faintly visible, which indicates that DLLE It can effectively inhibit the corrosion of copper in sulfuric acid solution.

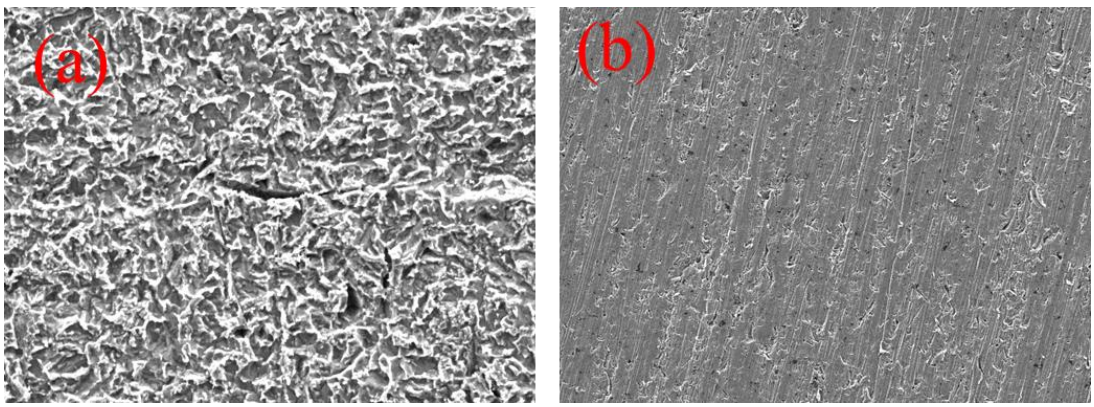

Figure 9. Surface topography of copper electrodes immersed in 0.5 M sulfuric acid solution with and without corrosion inhibitor at different concentrations.

4. CONCLUSION

The DLLE obtained by the acid extraction method contains a large number of oxygen-containing functional groups, which can exhibit high corrosion inhibition performance. The polarization curve data show that DLLE can simultaneously inhibit the reaction of the cathode and anode of the copper electrode,

which belongs to the mixed corrosion inhibitor. Electrochemical impedance spectroscopy data show that DLLE can greatly increase the charge transfer resistance after adsorption on the copper surface, showing high corrosion inhibition efficiency. Surface morphology test results show that DLLE can effectively inhibit the corrosion of copper in sulfuric acid solution after adsorption on copper surface. Both quantum chemical calculations and molecular dynamics simulations show that the active ingredients in DLLE can exhibit high corrosion inhibition performance.

References

1. K. J. Al-Sallami, *Int. J. Electrochem. Sci*., 16 (2021) 210929.
2. B. Tan, S. Zhang, Y. Qiang, L. Guo, L. Feng, C. Liao, Y. Xu, S. Chen, *J. Colloid Interf. Sci*., 526 (2018) 268.
3. D. Zheng, *Int. J. Electrochem. Sci*., 16 (2021) 210734.
4. G. E. Badr, *Int. J. Electrochem. Sci*., 16 (2021) 210832.
5. M.B.P. Mihajlović, M.M. Antonijević, *Int. J. Electrochem. Sci*., 10 (2015) 1027
6. B. Tan, S. Zhang, Y. Qiang, L. Feng, C. Liao, Y. Xu, S. Chen, *J. Mol.. Liq.*, 248 (2017) 902.
7. H. A. Alrafai, *Int. J. Electrochem. Sci*., 17 (2022) 220216.
8. S. Eid, *Int. J. Electrochem. Sci*., 16 (2021) 150852.
9. Z. Chen, *Int. J. Electrochem. Sci*., 16 (2021) 210559.
10. G. A. Gaber, *Int. J. Electrochem. Sci*., 16 (2021) 211214.
11. Z.Z. Tasic, M.M. Antonijevic, M.B. Petrovic Mihajlovic, M.B. Radovanovic, *J. Mol.. Liq.*, 219 (2016) 463.
12. M.B. Radovanovic, M.B. Petrovic, A.T. Simonovic, S.M. Milic, M.M. Antonijevic, *Sci. Pollut.Res. Int*., 20 (2013) 4370.
13. Y. Zhang, Y. Pan, P. Li, X. Zeng, B. Guo, J. Pan, L. Hou, X. Yin, *Colloid. Surface. A.*, 623 (2021) 126717.
14. B. Tan, J. He, S. Zhang, C. Xu, S. Chen, H. Liu, W. Li, *J. Colloid Interf. Sci.*, 585 (2021) 287.
15. Y. Feng, J. He, Y. Zhan, J. An, B. Tan, *J. Mol. Liq.*, 334 (2021) 116110.
16. L. Guo, B. Tan, W. Li, Q. Li, X. Zheng, I.B. Obot, *J. Mol. Liq.*, 327 (2021) 114828.
17. Y. Wu, L. Guo, Y. She, *J. Mol. Liq.*, 346 (2022) 117858.
18. Y. Zhou, C. Zhu, S. Xu, B. Xiang, R. Marzouki, *J. Ind. Eng. Chem.*, 102 (2021) 302.
19. Q. Xiang, J. He, *J. Mol. Liq.*, 325 (2021) 115218.
20. H. Chunyan, L. Jie, M. Jiani, X. Hui, J. Qingqing, *J. Chinese Med. Mater.*, 10 (2017) 2344.
21. B. Tan, S. Zhang, W. Li, X. Zuo, Y. Qiang, L. Xu, J. Hao, S. Chen, *J. Ind. Eng. Chem.*, 77 (2019) 449.
22. H. Movahedinia, *Int. J. Electrochem. Sci.*, 16 (2021) 210228.
23. B. Tan, S. Zhang, H. Liu, Y. Guo, Y. Qiang, W. Li, L. Guo, C. Xu, S. Chen, *J. Colloid Interf. Sci.*, 538 (2019) 519.
24. S. Singh, *Int. J. Electrochem. Sci*., 17 (2022) 220341.
25. A. S Al-Gorair, *Int. J. Electrochem. Sci*., 16 (2021) 210771.
26. Z.Z. Tasic, M.B.P. Mihajlovic, A.T. Simonovic, M.B. Radovanovic, M.M. Antonijevic, *Sci. Rep*., 9 (2019) 14710.
27. M.B. Petrović Mihajlović, M.B. Radovanović, Ž.Z. Tasić, M.M. Antonijević, *J. Mol. Liq*., 225 (2017) 127.
28. M.B. Radovanovic, M.M. Antonijevic, *J. Mater. Eng. Perform*., 25 (2016) 921.
29. B. Tan, S. Zhang, H. Liu, Y. Qiang, W. Li, L. Guo, S. Chen, *J. Taiwan Inst. Chem. E*., 102 (2019) 424.

30. A. Toghan, *Int. J. Electrochem. Sci*., 16 (2021) 211118.
31. B. Tan, B. Xiang, S. Zhang, Y. Qiang, L. Xu, S. Chen, J. He, *J. Colloid Interf. Sci.*, 582 (2021) 918.
32. R. S. Abdel Hameed, *Int. J. Electrochem. Sci*., 16 (2021) 210446.
33. B. Tan, S. Zhang, Y. Qiang, W. Li, H. Liu, C. Xu, S. Chen, *J. Mol. Liq*., 286 (2019).
34. M. Zhang, *Int. J. Electrochem. Sci*., 16 (2021) 21042.
35. W. Zhang, C. Li, W. Wang, B. Li, X. Liu, Y. Liu, H. Guo, S. Chen, Y. Feng, Colloid. Surface. A. 637 (2022) 128199.
36. B. Tan, S. Zhang, Y. Qiang, W. Li, H. Li, L. Feng, L. Guo, C. Xu, S. Chen, G. Zhang, *J. Mol. Liq*., 298 (2020) 111975.
37. S. Singh, *Int. J. Electrochem. Sci*., 16 (2021) 210841.
38. B. Tan, W. Lan, S. Zhang, H. Deng, Y. Qiang, A. Fu, Y. Ran, J. Xiong, R. Marzouki, W. Li, *Colloids and Surfaces A: Physicochemical and Engineering Aspects*., 645 (2022) 128892.
39. J. He, Q. Xu, G. Li, Q. Li, R. Marzouki, W. Li, *J. Ind. Eng. Chem*., 102 (2021) 260.
40. J. He, D. Yu, Q. Xu, G. Li, G. Chen, J. An, J. Yang, W. Li, *J. Mol. Liq*. 325 (2021) 115145.
41. B. Tan, S. Zhang, J. He, W. Li, Y. Qiang, Q. Wang, C. Xu, S. Chen, *J. Mol. Liq*., 321 (2021) 114464.
42. J. Shen, D. Yang, L. Ma, Z. Gao, A. Yan, Q. Liao, *Colloids and Surfaces A: Physicochemical and Engineering Aspects*., 636 (2022) 128058.
43. B. Tan, S. Zhang, X. Cao, A. Fu, L. Guo, R. Marzouki, W. Li, *J. Colloid Interf. Sci*., 609 (2022) 838.
44. E. Berdimurodov, A. Kholikov, K. Akbarov, L. Guo, S. Kaya, K.P. Katin, D.K. Verma, M. Rbaa, O. Dagdag, R. Haldhar, *Colloids and Surfaces A*., 637 (2022) 128207.
45. W. Zhang, H. Li, Y. Liu, D. Wang, L. Chen, L. Xie, L. Li, W. Zhang, Y. Wu, *Colloids and Surfaces A*., 612 (2021) 126010